

Insights on the Mechanism of Action of INH-C₁₀ as an Antitubercular Prodrug

Diogo Vila-Viçosa,[†] Bruno L. Victor,[†] Jorge Ramos,[‡] Diana Machado,[‡] Miguel Viveiros,[‡] Jacek Switala,[§] Peter C. Loewen,[§] Ruben Leitão,^{†,||} Filomena Martins,^{*,†} and Miguel Machuqueiro^{*,†}

[†]Centro de Química e Bioquímica, Departamento de Química e Bioquímica, Faculdade de Ciências, Universidade de Lisboa, 1749-016 Lisboa, Portugal

[‡]Unidade de Microbiologia Médica, Instituto de Higiene e Medicina Tropical, Universidade Nova de Lisboa, 1349-008 Lisboa, Portugal

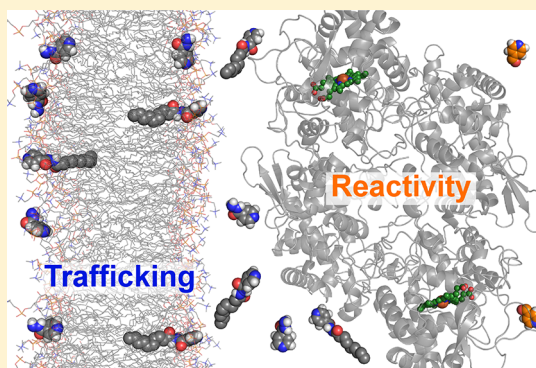
[§]Department of Microbiology, University of Manitoba, Winnipeg, Manitoba R3T 2N2, Canada

^{||}Área Departamental de Engenharia Química, Instituto Superior de Engenharia de Lisboa, Instituto Politécnico de Lisboa, R. Conselheiro Emídio Navarro, 1, 1959-007, Lisboa, Portugal

Supporting Information

ABSTRACT: Tuberculosis remains one of the top causes of death worldwide, and combating its spread has been severely complicated by the emergence of drug-resistance mutations, highlighting the need for more effective drugs. Despite the resistance to isoniazid (INH) arising from mutations in the *katG* gene encoding the catalase-peroxidase KatG, most notably the S315T mutation, this compound is still one of the most powerful first-line antitubercular drugs, suggesting further pursuit of the development of tailored INH derivatives. The *N'*-acylated INH derivative with a long alkyl chain (INH-C₁₀) has been shown to be more effective than INH against the S315T variant of *Mycobacterium tuberculosis*, but the molecular details of this activity enhancement are still unknown. In this work, we show that INH *N'*-acylation significantly reduces the rate of production of both isonicotinoyl radical and isonicotinyl-NAD by wild type KatG, but not by the S315T variant of KatG mirroring the *in vivo* effectiveness of the compound. Restrained and unrestrained MD simulations of INH and its derivatives at the water/membrane interface were performed and showed a higher preference of INH-C₁₀ for the lipidic phase combined with a significantly higher membrane permeability rate (27.9 cm s⁻¹, compared with INH-C₂ or INH (3.8 and 1.3 cm s⁻¹, respectively). Thus, we propose that INH-C₁₀ is able to exhibit better minimum inhibitory concentration (MIC) values against certain variants because of its better ability to permeate through the lipid membrane, enhancing its availability inside the cell. MIC values of INH and INH-C₁₀ against two additional KatG mutations (S315N and D735A) revealed that some KatG variants are able to process INH faster than INH-C₁₀ into an effective antitubercular form (*wt* and S315N), while others show similar reaction rates (S315T and D735A). Altogether, our results highlight the potential of increased INH lipophilicity for treating INH-resistant strains.

KEYWORDS: tuberculosis, KatG, mutation, activation, membrane



INTRODUCTION

According to WHO Global Tuberculosis Report 2016, tuberculosis (TB) was one of the top 10 causes of death worldwide in 2015 and was responsible for more deaths than HIV and malaria together. In fact, the 2015 figures—1.8 million deaths and 10.4 million people falling ill—speak for themselves.¹ In spite of this gloomy scenario, TB is a treatable and curable disease and, between 2000 and 2015, ca. 49 million lives were saved through TB diagnosis and appropriate treatment.¹ However, TB still occurs in every part of the world, with a higher incidence in low- and middle-income countries in Asia and Africa, where more than 95% of all deaths take place. One of the most serious threats to an effective control of TB epidemic lies in the global upsurge of

cases of multidrug and extensively drug-resistant forms of TB (MDR- and XDR-TB), nonresponsive to first-line drugs (at least isoniazid, INH, and rifampicin, RIF) or, concomitantly, also to the most effective second-line available antitubercular drugs, respectively.² Two new drugs, bedaquiline and delamanid, have recently received conditional approval by American, European, and Japanese regulatory agencies, and are now being used, one or the other, as part of new, long, but not totally exempted from side

Received: August 21, 2017

Revised: October 27, 2017

Accepted: November 1, 2017

Published: November 1, 2017

effects, MDR-TB combination regimens.^{3,4} Various antitubercular drug treatment trials have been carried out to evaluate combinations of new, repurposed, and/or existing drugs. However, there is still no satisfactory solution leading to a shorter, safer, and effective treatment, particularly against MDR TB,³ and new drugs are urgently needed.

Despite the problems of resistance, INH, originally synthesized in the early 1950s, remains one of the two most powerful first-line anti-TB medicines, alongside RIF, and remains one of the pillars of all recommended WHO multidrug regimens.¹ Therefore, tailoring INH to develop derivatives with improved activity that might at the same time circumvent resistance, particularly in mutant strains, has become both a scientific and a social challenge.⁵

INH resistance has been associated with multiple genes, but the majority (64%) of all phenotypic INH resistance among *Mycobacterium tuberculosis* (*Mtb*) isolates is associated with *katG*,^{6–8} with the most common variant being a serine to threonine change at residue 315, S315T (93.4%), followed by that of serine to asparagine, S315N (3.6%).⁷ INH is in fact a prodrug that must first be activated by conversion to isonicotinyl–NAD (IN–NAD), in a process involving KatG. The protein facilitates formation of an isonicotinyl radical that reacts with NAD⁺ to generate an intermediate isonicotinyl–NAD radical that is subsequently reduced by superoxide to IN–NAD.^{5,6,9–19}

The efficiency with which KatG facilitates the formation of IN–NAD is reduced by certain specific mutations. In particular, the S315T variant of *Mtb* is highly INH resistant, but the reasons for this dramatic effect by a seemingly innocuous mutation are not yet fully understood despite several different explanations.^{17–32} Indeed, access to the heme pocket does not provide a consistent explanation for variations in INH susceptibility because the S315T mutation does not seem to create an enhanced barrier to entry,¹⁹ and removal of Asp141 (Asp137 in *Mtb* KatG) in *Burkholderia pseudomallei* (*Bp*) allows INH to enter and bind in the heme pocket but without a significant effect on INH activation.¹⁸ Furthermore, a binding site remote from the heme cavity has been identified in *Bp* KatG which correlates well with a putative electron transfer pathway to the heme for superoxide generation.³³ In addition, hints of additional remote binding sites have been suggested by crystal binding studies.^{18,34–37} Complicating the picture further, the *N'*-acylated INH, INH-C₁₀ (Figure 1), is 6× more effective against the

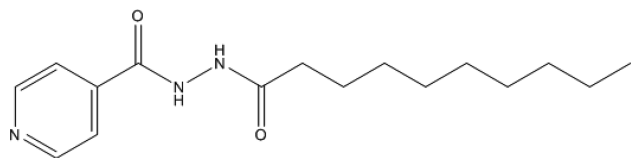


Figure 1. Schematic structure of INH-C₁₀.

S315T variant than INH (MIC values of 43.8 μM and 6.9 μM , for INH and INH-C₁₀, respectively), while retaining a similar activity in *wt* KatG (MIC values of 0.3 μM and 0.4 μM , for INH and INH-C₁₀, respectively).³⁸ Molecular docking studies with both INH and INH-C₁₀ on KatG heme pocket revealed only subtle differences in their modes of binding,¹⁹ suggesting that there may be other factors influencing the different activities observed for INH and its acylated derivatives.

In this work, we propose a multidisciplinary approach to investigate how and why INH-C₁₀ is able to outdo INH in the

S315T KatG mutation. We performed further MIC measurements in other KatG mutations to test for binding pocket effects. Rates of IN–NAD synthesis and IN[•] radical generation by KatG with INH and INH-C₁₀ were measured. Quantum mechanics (QM) calculations were carried out to assess the ability of acylated INH compounds to spontaneously form the IN[•] radical. MD simulations of INH and some acylated derivatives interacting with a model membrane were used to study how these compounds can permeate a lipid bilayer, thus allowing predictions on how they might reach KatG *in vivo*.

METHODS AND EXPERIMENTAL SECTION

Microbiology Studies. Wild-type strain *Mtb* H37Rv ATCC27294^T fully susceptible to INH (MIC = 0.04 mg L⁻¹–0.3 μM); *Mtb* S315T, mono-resistant to INH (MIC = 10 mg L⁻¹–43.8 μM ; *katG* S315T); MTB315N, resistant to streptomycin (SM^R, *rrs* S23A-C) and INH (INH MIC = 3 mg L⁻¹–21.9 μM ; *katG* S315N); and MTB735, multidrug resistant (MDR): INH^R (INH MIC = 80 mg L⁻¹–583.4 μM ; *katG* D735A) plus rifampicin resistant (RIF^R, *rpoB* S531L) and aminoglycoside amikacin resistant and capreomycin resistant (AMK^RCAP^R, *rrs* A1401G) were included in this study. These strains belong to the culture collection of the Grupo de Micobacterias, Unidade de Microbiologia Médica (IHMT/UNL), and the mutated strains were obtained from patients diagnosed with active TB in Lisbon in 2003, 2009, and 2011, respectively. Mutations in the structural *katG* gene and in the *inhA* promoter and regulatory region were characterized by DNA sequencing as previously described.³⁹ Cultures and MIC determination were conducted using the BACTEC MGIT 960 system (BACTEC 960) and the Epicenter VS.53A software equipped with the TB eXIST module (Becton Dickinson Diagnostic Systems, USA) as previously described.^{40,41}

For MIC determination, stock solutions of the compound were prepared in methanol (the most appropriate solvent to guarantee the adequate solubility of the compounds without any effect on the viability of the mycobacteria at the final volumes used) from Sigma-Aldrich (St. Louis, MO, USA), aliquoted, and stored at 253 K. On the day of the experiment, fresh working solutions were prepared using the same organic solvent, and the desired concentrations were prepared with sterilized distilled water. For INH, the concentrations used were as follows: sequential dilutions ranged from 0.01 to 12 mg L⁻¹, plus 20 to 160 mg L⁻¹. For INH-C₁₀, the concentrations used were as follows: 1.0, 3.0, 4.0, 6.0, 8.0, 10.0, and 20.0 mg L⁻¹. 0.1 mL of each tested concentration was inoculated in MGIT tubes containing 0.8 mL of SIRE supplement and 0.5 mL of the strain suspension. The compound-free growth control tube (proportional control) was inoculated with 0.5 mL of the culture diluted 1:100 with a sterile saline solution. Additionally, a second compound-free growth control containing 0.1 mL of methanol was inoculated with 0.5 mL of the undiluted suspension of the strain to serve as absolute control for inoculum errors and for any possible solvent effect on bacterial growth. Mycobacterial growth in the MGIT tubes was continuously monitored with the EpiCenter TB eXIST software. The interpretation of the results was performed as follows: when the compound-free proportional control tube reached a growth unit (GU) value of 400, the test was considered complete. If the GU of the compound-containing tube to be compared with is ≥ 100 , the strain was considered resistant; if the GU of the compound-containing tube is < 100 , the strain was considered susceptible to that concentration.⁴⁰ The MIC was defined as the lowest concentration necessary to

inhibit 99% of the bacterial population, corresponding to the compound-containing tube first recorded as susceptible. MIC determination was performed in triplicate and the final value given as the result of two concordant values.^{40,41}

Quantum Mechanics Calculations. Density functional theory calculations were performed using the GAUSSIAN 09 software package⁴² and the M06 functional⁴³ with the aug-cc-pVDZ Dunning basis sets.^{44,45} Frequency calculations were performed to confirm the absence of imaginary frequencies for the obtained minima. The Gibbs free energies of formation were calculated using a thermodynamic cycle based on the spontaneous activation of INH and its derivatives. As an example, we show the cycles for INH and INH-C₂.

$$\Delta G^{\text{INH}} = G(\text{I}^*) + G(\text{H}^+) + G(\text{e}^-) + G(\text{N}_2\text{H}_2) - G(\text{INH})$$

$$\Delta G^{\text{INH-C}_2} = G(\text{I}^*) + G(\text{H}^+) + G(\text{e}^-) + G(\text{N}_2\text{HAc}) - G(\text{INH-C}_2)$$

Therefore, comparing directly INH-C₂ with INH we get

$$\begin{aligned} \Delta \Delta G &= \Delta G^{\text{INH-C}_2} - \Delta G^{\text{INH}} = G(\text{I}^*) + G(\text{H}^+) + G(\text{e}^-) + G(\text{N}_2\text{HAc}) \\ &- G(\text{INH-C}_2) - G(\text{I}^*) - G(\text{H}^+) - G(\text{e}^-) - G(\text{N}_2\text{H}_2) + G(\text{INH}) \\ &= G(\text{N}_2\text{HAc}) - G(\text{INH-C}_2) - G(\text{N}_2\text{H}_2) + G(\text{INH}) \end{aligned}$$

For longer chain INH-C_n molecules, an analogous procedure was applied.

Radical Generation Kinetic Studies. The release of radicals from INH, INH-C₂, and INH-C₁₀ was assayed by the increase in absorbance at 560 nm caused by nitro blue tetrazolium reduction to formazan ($\epsilon = 18,500 \text{ M}^{-1} \text{ cm}^{-1}$)⁴⁶ in a solution containing 1.0 mM INH, 0.2 μM MnCl₂, 0.2 mM nitro blue tetrazolium, 50 mM Tris-HCl, pH 8.0, and 50% DMSO, at 37 °C. The synthesis of IN-NAD was assayed by the increase in absorbance at 326 nm ($\epsilon = 6,900 \text{ M}^{-1} \text{ cm}^{-1}$)¹⁴ of a solution containing 0.4 mM NAD⁺, 1.0 mM INH (also 1.0 mM INH-C₂ or INH-C₁₀, 2 μM MnCl₂), 50 mM Tris-HCl, pH 8.0, and 50% DMSO at 37 °C. The kinetic measurements were performed with *Bp* KatG, however, throughout this manuscript, we have used the corresponding residue numbering from *Mtb* KatG, for simplicity.

Rate constants for the production of IN-NAD radicals were calculated for each of the four systems (INH in *wt*, INH in mutant, INH-C₁₀ in *wt*, and INH-C₁₀ in mutant) using the Solver Microsoft Excel add-in. In each case, Solver was used to fit the nonlinearized first-order kinetic law ($P_t = P_\infty - A_0 e^{-kt}$) to the experimental absorbance *vs* time data, by adjusting simultaneously P_∞ , A_0 , and k so that the sum of the squared differences between P_{calc} and P_{exp} (χ^2) was minimized. P and A stand for product and reagent concentration, respectively, k represents the rate constant, t is the time, and the subscripts 0 and ∞ indicate the value of the property at $t = 0$ and $t = \infty$. As solving method, we chose GRG Nonlinear, with a constraint precision of 10^{-6} , and a convergence of 10^{-4} in the Multistart option (population size 1000 and random seed 10). For each system, different starting values were used for each adjusted parameter to maximize the probability that the found solution corresponded to the global minimum.

MD Simulations. Molecular mechanics/molecular dynamics (MM/MD) simulations were carried out in order to understand the structural preferences of INH, INH-C₂, and INH-C₁₀ at the water/membrane interface. We performed 6 sets of simulations (Table S1) placing the studied molecules at the center of a bilayer (in) or in water, near the bilayer interface (out).

A previously equilibrated membrane of 128 1-palmitoyl-2-oleoyl-*sn*-glycero-3-phosphocholine (POPC) lipids solvated

with 5941 water molecules was used to prepare all starting conformations. The simulations were carried out using the GROMACS 5.1 or GROMACS 2016.3 (PMF calculations) packages⁴⁷ and the GROMOS 54A7 force field^{48–50} together with the SPC water model.⁵¹ For INH, INH-C₂, and INH-C₁₀, the topologies were obtained from the Automated Topology Builder (ATB) and Repository^{52,53} and manually curated. The ATB topologies were modified in the pairs section in order to exclude 1–4 interactions in the pyridyl moiety, analogously to the GROMOS rules for aromatic rings. Due to the chemical similarity between INH-C₂ and INH-C₁₀, we propagated the INH-C₂ topology with the extra carbon tail to build INH-C₁₀. The conformational space was sampled according to a NPT ensemble where the pressure (1 bar with a coupling constant of 2 ps) and temperature (298.15 K with a coupling constant of 0.1 ps) were kept constant using the Parrinello–Rahman barostat^{54,55} and ν -rescale thermostat,⁵⁶ respectively. Semi-isotropic pressure coupling was used with a compressibility of $4.5 \times 10^{-5} \text{ bar}^{-1}$. The particle mesh Ewald method was used for the electrostatic interactions with a real space cutoff of 1.0 nm and a Fourier grid spacing of 0.12 nm. van der Waals interactions were truncated above 1.0 nm. All bonds were constrained using the P-LINCS algorithm⁵⁷ for membrane and solutes, and SETTLE⁵⁸ for water. The equations of motion were integrated every 2 fs with the neighbor lists being updated every 10 steps. A minimization and initiation protocol was performed in all systems to avoid unfavorable interactions. In the minimization step we used both steepest descent and low-memory Broyden–Fletcher–Goldfarb–Shanno algorithms. The initiation was performed in two steps of 100 ps each: the first was performed at constant volume and the second with a temperature coupling constant of 0.01 ps to avoid large fluctuations.

In the INH^{out}, INH-C₂^{out}, and INH-C₁₀^{out} simulations all 50 ns was used for analysis. In the other 3 sets, initial periods of different sizes were discarded to allow for an adequate equilibration of the compound position relative to the lipid molecules (Table S2).

In the potential of mean force (PMF) simulations, we built 36 initial structures for the umbrellas by pulling each compound across the lipid bilayer (at 1 nm ns^{-1} with a force constant of $10^3 \text{ kJ mol}^{-1} \text{ nm}^{-2}$). We selected equally spaced windows (in intervals of 0.1 nm) ranging from the center of the bilayer (0 nm) to a distance of 3.5 nm (zero energy setting), corresponding to bulk water. Each umbrella was 100 ns long, and the last 80 ns was used in the PMF calculation where the compound is restrained using a bias force constant of $10^3 \text{ kJ mol}^{-1} \text{ nm}^{-2}$ centered in the N' atom. The weighted histogram analysis method (WHAM)⁵⁹ was used for the PMF calculations. The error bars were calculated using 50 bootstrap calculations in the Bayesian histogram bootstrapping method. The permeability rates were calculated using the inhomogeneous solubility–diffusion model (ISDM)^{60,61} coupled to the biasing harmonic potential.^{62,63}

Pymol software (Schrödinger) was used for structure visualization and image rendering.

RESULTS AND DISCUSSION

In a previous work, we showed that INH-C₁₀ is 6× more effective than INH against the common INH^R S315T mutant of *Mtb*,³⁸ and, in this paper, we report an investigation of the phenomenon and present an explanation for the unique effectiveness of INH-C₁₀. A summary of the working hypothesis arising from the present study is shown in Figure 2. We propose that the production of IN• radical, the intermediate required for IN–

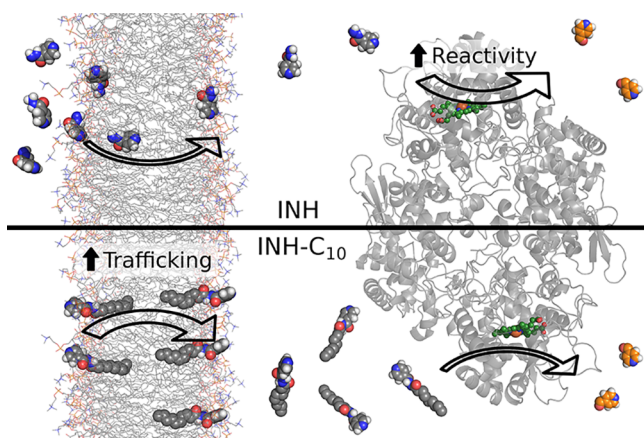


Figure 2. Overall scheme illustrating INH (top) and INH-C₁₀ (bottom) trafficking (in a POPC membrane) and reactivity (in KatG). Both POPC membrane and KatG are shown in light gray, with the heme groups depicted as small green spheres. INH and INH-C₁₀ carbon atoms are shown as darker gray spheres, while the isonicotinoyl radicals are depicted as orange spheres.

NAD synthesis, depends on (1) prodrug trafficking through the cell membrane (which includes contributions from all interactions exhibited by the compounds until they reach the target); (2) the levels of KatG in the cell, which will vary depending on gene expression and folding of the nascent protein into an active structure; and (3) the reactivity of KatG toward the prodrug, which will depend on the prodrug structure and on the activity of KatG as affected by mutation. Data in support of this working proposal are presented, and the discussion will often call back this scheme.

MIC Measurements. We have previously reported the MIC values for INH and INH-C₁₀ against *wt* and the S315T mutant of *Mtb*, which revealed that while the two were equally effective against the *wt* strain, INH-C₁₀ was 6× more effective against the S315T mutant.³⁸ In this work, we have measured the MIC values for INH and INH-C₁₀ against two new KatG mutations, one near the heme pocket (S315N), which is directly comparable to our previously studied S315T, and a second (D735A) located remote from the heme pocket (~25 Å, see Figure S1). The mutation at position 735, despite conferring the highest level of resistance to INH in *Mtb*, was included in this study because this mutation should not influence the steric or electrostatic interactions between the protein and INH or INH-C₁₀. Such a mutation should only have an indirect effect as a result of perturbations in protein folding leading to less protein or less active protein which is probably the reason for the significantly higher MIC values for both INH and INH-C₁₀ compared to the other mutants (Table 1). However, the lower MIC value (68.6 μM) of INH-C₁₀ compared with INH (583.4 μM), a proportional difference similar to that observed for S315T, is not trivial. The appearance of streptomycin resistance in S315N and of multidrug resistance in D735A is the result of additional mutations in *rms* (both strains) and in *rpoB* in D735A. However, the differences in effectiveness between INH and INH-C₁₀ among the different strains poses interesting questions. For example, why is INH-C₁₀ more effective against such different mutants S315T and D735A and not against S315N? And why do INH and INH-C₁₀ exhibit equal effectiveness against *wt* and S315N? These questions are addressed in the subsequent sections.

Effect of Acylation upon Spontaneous IN[•] Radical Formation. INH undergoes spontaneous breakdown in

Table 1. Experimental MIC Values against *Wt* and Different KatG Mutations^a

<i>Mtb</i> strain	KatG mutation	phenotype	MIC/μM	
			INH	INH-C ₁₀
<i>wt</i>			0.3	0.4
MTB315T	S315T	INH ^R	43.8	6.9
MTB315N	S315N	INH ^R , STR ^R	21.9	20.6
MTB735	D735A	MDR	583.4	68.6

^aThe values from *wt* and S315T mutation are from the literature.³⁸ Values from S315N and D735A mutations were obtained in this work. INH^R: INH resistant. STR^R: streptomycin resistant. MDR: multidrug resistant.

aqueous solution to diimide (H–N=N–H), H⁺, an electron, and the isonicotinoyl radical (IN[•]). This reaction is slow but still sufficiently fast that it presents a significant background in assays of KatG-generated IN[•], making a background correction essential.^{22,64} *N*-acylation of INH greatly reduces the spontaneous formation of radical species resulting in effectively no measurable radicals being produced from either INH-C₂ or INH-C₁₀, suggesting that the acylated hydrazide linkage is much more stable (Figure 3). Figure 4 shows the products that are expected

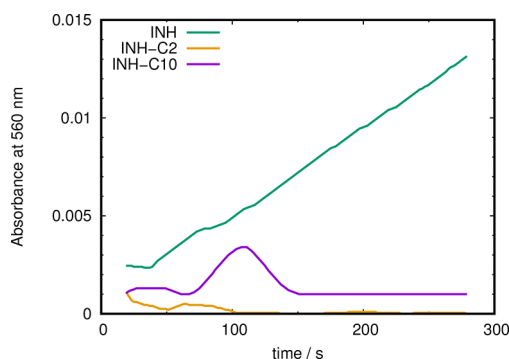


Figure 3. Free radical production assayed by the nitroblue tetrazolium (NBT) reduction reaction.

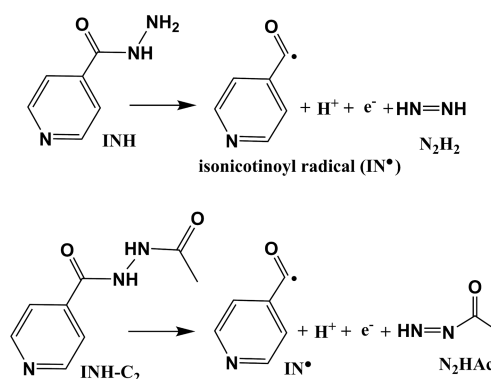


Figure 4. Scheme with products obtained from spontaneous activation of INH (top) and INH-C₂ (bottom).

from the spontaneous breakdown of INH and INH-C₂. It should be noted that these assays were carried out in 50% DMSO to ensure solubility of the acylated derivatives.

The Gibbs free energy of formation of the radicals from INH and the acylated INH derivatives was calculated (Table 2), and the positive ΔΔG values obtained for the derivatives confirm that the radical formation in these compounds is thermodynamically

Table 2. IN[•] Radical Gibbs Free Energies of Formation Obtained for INH and Its Acylated Derivatives^a

	$\Delta\Delta G$ (kcal mol ⁻¹)	bond length (Å)	Mayer bond order
INH	0.0	1.347	1.156
INH-C ₂	9.1	1.347	1.269
INH-C ₄	9.8	1.346	1.241
INH-C ₆	8.9	1.347	1.225
INH-C ₈	10.3	1.348	1.211
INH-C ₁₀	10.7	1.347	1.206

^aThe C–N bond lengths and Mayer bond orders are also shown.

less favored than in INH. The differences of approximately 10 kcal mol⁻¹ are significantly beyond the methodology uncertainties and make it clear that the size of the acyl group does not influence the energy balance between reactants and products. Furthermore, the acylation of INH does not influence the C–N bond lengths, even though it seems to slightly increase the Mayer bond order parameters by comparison with the parent compound, INH, suggesting a higher stability in that bond for the derivatives. These results are in good agreement with the spontaneous formation of the IN[•] radical in a purely aqueous buffer solution or in a 50% DMSO buffer solution from INH and not from INH-C₂ or INH-C₁₀ (Figure 3).⁵ Clearly, differences in the Gibbs free energies of formation of this magnitude will have influence over the KatG-catalyzed reaction as well.

Kinetics of KatG-Catalyzed IN[•] Formation. The spontaneous breakdown of INH to IN[•] is too slow to support the generation of IN–NAD at a sufficient rate to produce effective concentrations to elicit an antitubercular effect. Therefore, the rates of IN[•] radical formation in the presence of KatG were determined (Figure 5A).

The results confirm that INH is a better substrate for KatG, resulting in a significantly larger yield of radicals than either of its acylated derivatives, INH-C₁₀ yielding slightly more than INH-C₂. Interestingly, the S315T variant of KatG generates radicals at a slower rate from INH than does the native enzyme, but generates radicals faster from INH-C₂ and INH-C₁₀. The more specific assay for isonicotinoyl radical, its reaction with NAD⁺ (Figure 5B), confirmed that INH is a much better radical source than INH-C₁₀ using *wt* KatG (the first order rate constants are provided in Table 3), but with the S315T variant of KatG, the rates of IN–NAD synthesis from INH and INH-C₁₀ are the same. Moreover, S315T variant produces IN–NAD faster from INH-C₁₀ than does native KatG. The discrepancy between the 4× faster synthesis of IN–NAD from INH compared to INH-C₁₀ and the similar MIC values of 0.3 and 0.4 is striking and suggests that another factor is affecting the reaction. One likely possibility pursued in the next section is that of trafficking.

Trafficking of INH and Its Derivatives To Reach KatG.

The cell wall with its sheath of mycolic acids and the lipid bilayer membrane present barriers to the entry of INH (and its derivatives) into the cell prior to reaching KatG. It is unclear if transport involves simple passive diffusion or occurs via an as yet unidentified transport system. In both scenarios, associations with the cell wall and the membrane are to be expected. Modeling the interaction of INH derivatives with the cell wall is not feasible because of its complicated and variable structure, but it is possible to model and compare the interactions of INH and its derivatives with a lipid bilayer. Short INH^{out}, INH-C₂^{out}, and INH-C₁₀^{out} simulations (50 ns) were performed to evaluate the preferred positions of these compounds near the water/membrane interface. In these simulations, all molecules

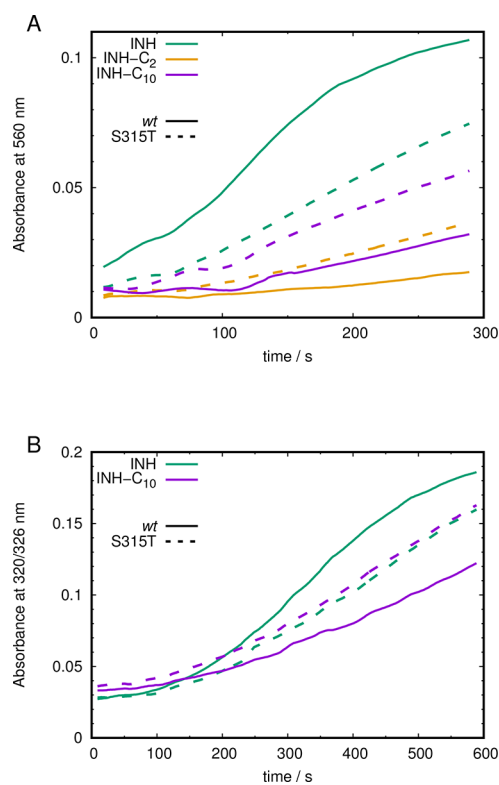


Figure 5. Isonicotinoyl radical formation measured using the NBT assay (A) and the IN–NAD adduct formation (B) in the presence of INH and its acylated derivatives for *wt* and S315T KatG (*Mtb* numbering is used, although experiments were performed with *Bp* KatG). Floating window averages of the absorbance data are shown for clarity.

Table 3. First Order Rate Constants (*k*), Correlation Coefficient of P_{calc} vs P_{exp} (r^2), and χ^2 for *Wt* and S315T KatG Producing IN–NAD Adduct from INH and INH-C₁₀

KatG	INH			INH-C ₁₀		
	$10^3k/s^{-1}$	r^2	χ^2	$10^3k/s^{-1}$	r^2	χ^2
<i>wt</i>	2.70	0.999	6.6×10^{-5}	0.65	0.991	4.3×10^{-4}
S315T	1.09	0.997	4.9×10^{-4}	1.01	0.997	2.7×10^{-4}

interacted with the bilayer in a relatively short time scale (Figures S2 and S3). INH-C₂ and INH-C₁₀ pyridyl rings clearly prefer to interact with lipid head groups remaining at the interface most of the simulation time (only one desorption event was observed in replicate 2 for INH-C₂). This observation is probably related to the alkyl groups of INH-C₂ and INH-C₁₀, which act as an anchor promoting accumulation in the membrane. On the other hand, INH, despite being also observed at the interface, is often completely solvated indicating a lower membrane affinity.

Long INHⁱⁿ, INH-C₂ⁱⁿ, and INH-C₁₀ⁱⁿ simulations (500 ns) were performed to achieve equilibrium and characterize the system's conformational space. Starting from the center of the bilayer, the compounds converged more rapidly to their preferred positions (INH-C₂ and INH-C₁₀ at the interface and INH exchanging between the solvent and the interface). These preferred positions (Figure 6) are in agreement in all replicates independently of the starting conformations, which means that the system is not energy trapped.

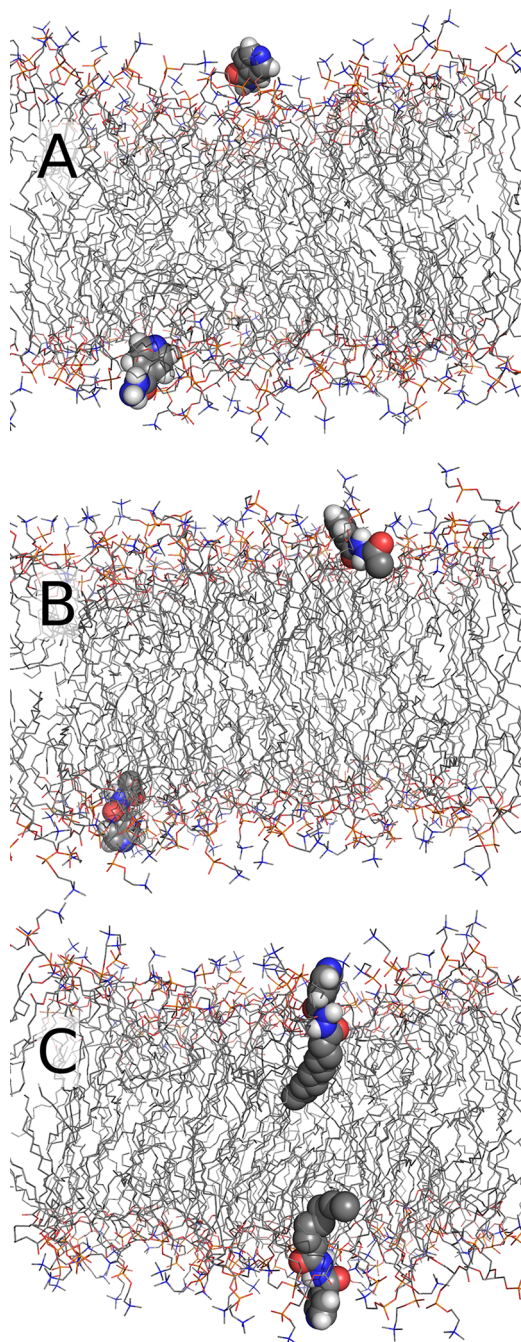


Figure 6. Representative conformations of INH (A), INH-C₂ (B), and INH-C₁₀ (C) preferred positions in the membrane. Compounds are shown as spheres with dark gray carbons. POPC lipids are depicted as thin sticks for clarity.

After the equilibration period, INH, INH-C₂, and INH-C₁₀ pyridyl rings show higher abundance at the interface (Figure 7). The distribution of INH along the membrane normal is slightly wider, probably due to its smaller size and lower lipophilicity. Nevertheless, the significant lipid interaction probability observed for this compound is overestimated in our simulations due to a limited box size. The relatively small number of water molecules, used to speed up computer simulations, substantially underestimates the fraction of INH conformations in this phase, since the compound is always near the membrane. INH derivatives are not subject to this entropic effect as they do not exchange between phases in our long simulations. Both INH-C₂

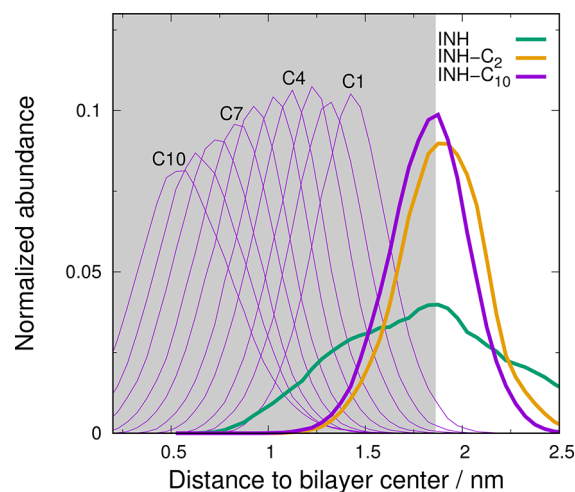


Figure 7. Distance to bilayer center histograms of key atoms in INH, INH-C₂, and INH-C₁₀. The thick lines correspond to the carbon atoms in the *para* position of the pyridyl rings. The thin lines represent the carbon atoms of the INH-C₁₀ aliphatic tail. For C1 and C2 of INH-C₂, similar distributions were observed. The gray shaded area corresponds to the membrane region (below the phosphorus atom's average position).

and INH-C₁₀ adopt a vertical position aligned with the membrane normal (carbon atom position distributions are shown in Figure 7), intercalating its acyl chain with the lipidic tails (Figures 6B and 6C). However, the difference in the experimental octanol/water log*P* values between the two compounds (-0.9 for INH-C₂ and 3.5 for INH-C₁₀⁶⁵) indicates that INH-C₁₀ should favor the lipidic phase compared with INH-C₂. We used potential of mean force (PMF) calculations to estimate the preferred bilayer regions of these compounds and their membrane permeability rates (Figure 8). The free energy profiles show a minimum at the 1.5–1.9 nm region (for the *N'*-acyl atom) corresponding to the water/membrane interface preferred positions (Figure 6). The depth of these minima (~ -1

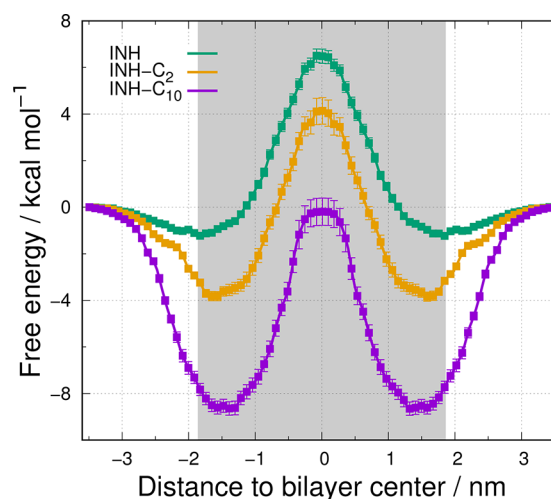


Figure 8. Free energy profiles associated with the complete permeation process of INH, INH-C₂, and INH-C₁₀ across a POPC lipid bilayer. The PMF was calculated for one leaflet, and the other one was assumed to be identical by symmetry. The ISDM^{62,63} permeability rates obtained from these simulations are 1.3, 3.8, and 27.9 cm s⁻¹, for INH, INH-C₂, and INH-C₁₀, respectively.

for INH, ~ -4 for INH-C₂, and ~ -9 kcal mol⁻¹ for INH-C₁₀) is a proper estimation of the compounds' relative lipophilicities. In fact, they roughly agree with the experimental octanol/water log*P* values. The difference among these minima also indicates that INH-C₁₀ accumulates more in the lipidic phase than INH-C₂, emphasizing the key role of the larger acyl chain. Using the bias simulations, we estimated the ISDM^{62,63} permeability rates (Figure S4) of these compounds in the POPC bilayer (1.3, 3.8, and 27.9 cm s⁻¹, for INH, INH-C₂, and INH-C₁₀, respectively). The 1 order of magnitude higher permeability rate for INH-C₁₀ suggests that it crosses more easily the lipidic membrane thereby facilitating a more rapid transport into the cell.

CONCLUSIONS

In this work, we have shown that *N'*-acylated INH derivatives can be more effective against certain *Mtb* mutants such as S315T and D735A than INH itself and an investigation of the differential effect is described. The *N'*-acyl group stabilizes the molecule, resulting in slower spontaneous IN[•] radical formation. KatG facilitates IN[•] formation, and, whereas INH is the preferred substrate for the *wt* enzyme, INH-C₁₀ is the preferred substrate for the S315T variant. MD simulations show that INH-C₁₀ accumulates in the membrane and exhibits a high membrane crossing rate, possibly enhancing trafficking and leading to a higher intracellular concentration, which compensates for its lower reactivity. Also, in KatG mutations, it is possible that the amount of expressed protein is lower than in *wt*, which helps to rationalize the higher MIC values. This means that more reactive drugs with better trafficking properties are needed to counterbalance the observed limitations.

The several pieces of evidence presented provide new insights toward a deeper rationalization of the experimental MIC values obtained for these compounds in various strains of *Mtb*. The development of INH derivatives with increased activity against S315T mutants, the worldwide most prevalent INH resistance related mutation, is a promising area for antitubercular drug development that extends and leverages the therapeutic usefulness of INH, rather than replacing it in MDR-TB therapeutics by options that are less effective and more toxic. Overall, our results encourage the search for new INH-based antitubercular derivatives with improved trafficking and reactivity profiles, and prompt researchers to also test their compounds in KatG mutations.

ASSOCIATED CONTENT

Supporting Information

The Supporting Information is available free of charge on the ACS Publications website at DOI: 10.1021/acs.molpharmaceut.7b00719.

MD simulation summary and equilibration times, snapshot of KatG, membrane insertion over time, representative snapshots, and local PMF, diffusion, and resistance profiles (PDF)

AUTHOR INFORMATION

Corresponding Authors

*E-mail: filomena.martins@fc.ul.pt. Phone: +351-21-7500870. Fax: +351-21-7500088.

*E-mail: machuque@ciencias.ulisboa.pt. Phone: +351-21-7500112. Fax: +351-21-7500088.

ORCID

Peter C. Loewen: 0000-0003-4507-4356

Miguel Machuqueiro: 0000-0001-6923-8744

Notes

The authors declare no competing financial interest.

ACKNOWLEDGMENTS

The authors would like to thank Prof. Susana Santos for the purification of INH-C₂ and INH-C₁₀. This work was supported by Grant RGPIN9600 from the Natural Sciences and Engineering Research Council (NSERC) of Canada (to P.C.L.) and the Canada Research Chair Program (to P.C.L.). Financial support from Fundação para a Ciência e a Tecnologia, Portugal, under Grants PTDC/QEQ-COM/5904/2014, UID/MULTI/00612/2013, UID/MULTI/04413/2013, SFRH/BPD/100688/2014, and SFRH/BPD/110491/2015 is also greatly appreciated.

REFERENCES

- (1) World Health Organization. *Global Tuberculosis Report 2016*. http://www.who.int/tb/publications/global_report/en/ (accessed: Feb 28, 2017).
- (2) World Health Organization. *WHO Factsheet on MDR*. http://www.who.int/tb/challenges/mdr/mdr_tb_factsheet.pdf (accessed: Feb 28, 2017).
- (3) Zumla, A.; Chakaya, J.; Centis, R.; D'Ambrosio, L.; Mwaba, P.; Bates, M.; Kapata, N.; Nyirenda, T.; Chanda, D.; Mfinanga, S.; Hoelscher, M.; Maeurer, M.; Migliori, G. Tuberculosis treatment and management—an update on treatment regimens, trials, new drugs, and adjunct therapies. *Lancet Respir. Med.* **2015**, *3*, 220–234.
- (4) Brigden, G.; Hewison, C.; Varaine, F. New developments in the treatment of drug-resistant tuberculosis: clinical utility of bedaquiline and delamanid. *Infect. Drug Resist.* **2015**, *8*, 367.
- (5) Martins, F.; Ventura, C.; Santos, S.; Viveiros, M. QSAR Based Design of New Antitubercular Compounds: Improved Isoniazid Derivatives against Multidrug-Resistant TB. *Curr. Pharm. Des.* **2014**, *20*, 4427–4454.
- (6) Zhang, Y.; Heym, B.; Allen, B.; Young, D.; Cole, S. The catalase–peroxidase gene and isoniazid resistance of *Mycobacterium tuberculosis*. *Nature* **1992**, *358*, 591–593.
- (7) Seifert, M.; Catanzaro, D.; Catanzaro, A.; Rodwell, T. C. Genetic mutations associated with isoniazid resistance in *Mycobacterium tuberculosis*: a systematic review. *PLoS One* **2015**, *10*, e0119628.
- (8) Dominguez, J.; Boettger, E.; Cirillo, D.; Cobelens, F.; Eisenach, K.; Gagneux, S.; Hillemann, D.; Horsburgh, R.; Molina-Moya, B.; Niemann, S.; Tortoli, E.; Whitelaw, A.; Lange, C. TBNET and RESIST-TB networks, Clinical implications of molecular drug resistance testing for *Mycobacterium tuberculosis*: a TBNET/RESIST-TB consensus statement. *Int. J. Tuberc. Lung Dis.* **2016**, *20*, 24–42.
- (9) Welinder, K. G. Superfamily of plant, fungal and bacterial peroxidases. *Curr. Opin. Struct. Biol.* **1992**, *2*, 388–393.
- (10) Heym, B.; Zhang, Y.; Poulet, S.; Young, D.; Cole, S. Characterization of the katG gene encoding a catalase-peroxidase required for the isoniazid susceptibility of *Mycobacterium tuberculosis*. *J. Bacteriol.* **1993**, *175*, 4255–4259.
- (11) Quemard, A.; Dessen, A.; Sugantino, M.; Jacobs, W. R., Jr.; Sacchettini, J. C.; Blanchard, J. S. Binding of catalase-peroxidase-activated isoniazid to wild-type and mutant *Mycobacterium tuberculosis* enoyl-ACP reductases. *J. Am. Chem. Soc.* **1996**, *118*, 1561–1562.
- (12) Rozwarski, D. A.; Grant, G. A.; Barton, D. H. R.; Jacobs, W. R., Jr.; Sacchettini, J. C. Modification of the NADH of the isoniazid target (InhA) from *Mycobacterium tuberculosis*. *Science* **1998**, *279*, 98–102.
- (13) Scior, T.; Morales, I. M.; Eisele, S. J. G.; Domeyer, D.; Laufer, S. Antitubercular isoniazid and drug resistance of *Mycobacterium tuberculosis*: a review. *Arch. Pharm.* **2002**, *335*, 511–525.
- (14) Rawat, R.; Whitty, A.; Tonge, P. J. The isoniazid-NAD adduct is a slow, tight-binding inhibitor of InhA, the *Mycobacterium tuberculosis* enoyl reductase: adduct affinity and drug resistance. *Proc. Natl. Acad. Sci. U. S. A.* **2003**, *100*, 13881–13886.

- (15) Timmins, G. S.; Deretic, V. Mechanisms of action of isoniazid. *Mol. Microbiol.* **2006**, *62*, 1220–1227.
- (16) Vilchêze, C.; Jacobs, W. R., Jr. The mechanism of isoniazid killing: clarity through the scope of genetics. *Annu. Rev. Microbiol.* **2007**, *61*, 35–50.
- (17) Wiseman, B.; Carpena, X.; Feliz, M.; Donald, L. J.; Pons, M.; Fita, I.; Loewen, P. C. Isonicotinic acid hydrazide conversion to isonicotinyl-NAD by catalase-peroxidases. *J. Biol. Chem.* **2010**, *285*, 26662–26673.
- (18) Vidossich, P.; Loewen, P. C.; Carpena, X.; Fiorin, G.; Fita, I.; Rovira, C. Binding of the Antitubercular Pro-Drug Isoniazid in the Heme Access Channel of Catalase-Peroxidase (KatG). A Combined Structural and Metadynamics Investigation. *J. Phys. Chem. B* **2014**, *118*, 2924–2931.
- (19) Teixeira, V. H.; Ventura, C.; Leitão, R.; Ráfols, C.; Bosch, E.; Martins, F.; Machuqueiro, M. Molecular Details of INH–C10 Binding to *wt* KatG and Its S315T Mutant. *Mol. Pharmaceutics* **2015**, *12*, 898–909.
- (20) Heym, B.; Alzari, P. M.; Honore, N.; Cole, S. T. Missense mutations in the catalase-peroxidase gene, *katG*, are associated with isoniazid resistance in *Mycobacterium tuberculosis*. *Mol. Microbiol.* **1995**, *15*, 235–245.
- (21) Wengenack, N. L.; Todorovic, S.; Yu, L.; Rusnak, F. Evidence for differential binding of isoniazid by *Mycobacterium tuberculosis* KatG and the isoniazid-resistant mutant KatG (S315T). *Biochemistry* **1998**, *37*, 15825–15834.
- (22) Wengenack, N. L.; Rusnak, F. Evidence for Isoniazid-Dependent Free Radical Generation Catalyzed by *Mycobacterium tuberculosis* s KatG and the Isoniazid-Resistant Mutant KatG (S315T). *Biochemistry* **2001**, *40*, 8990–8996.
- (23) Powers, L.; Hillar, A.; Loewen, P. C. Active site structure of the catalase-peroxidases from *Mycobacterium tuberculosis* and *Escherichia coli* by extended X-ray absorption fine structure analysis. *Biochim. Biophys. Acta, Protein Struct. Mol. Enzymol.* **2001**, *1546*, 44–54.
- (24) Yamada, Y.; Fujiwara, T.; Sato, T.; Igarashi, N.; Tanaka, N. The 2.0 Å crystal structure of catalase-peroxidase from *Haloarcula marismortui*. *Nat. Struct. Biol.* **2002**, *9*, 691–695.
- (25) Carpena, X.; Loprasert, S.; Mongkolsuk, S.; Switala, J.; Loewen, P.; Fita, I. Catalase-peroxidase KatG of *Burkholderia pseudomallei* at 1.7 Å resolution. *J. Mol. Biol.* **2003**, *327*, 475–489.
- (26) Bertrand, T.; Eady, N.; Jones, J.; Jesmin; Nagy, J.; Jamart-Grégoire, B.; Raven, E.; Brown, K. Crystal structure of *Mycobacterium tuberculosis* catalase-peroxidase. *J. Biol. Chem.* **2004**, *279*, 38991–38999.
- (27) Deemagarn, T.; Carpena, X.; Singh, R.; Wiseman, B.; Fita, I.; Loewen, P. C. Structural Characterization of the Ser324Thr Variant of the Catalase-peroxidase (KatG) from *Burkholderia pseudomallei*. *J. Mol. Biol.* **2005**, *345*, 21–28.
- (28) Zhao, X.; Yu, H.; Yu, S.; Wang, F.; Sacchettini, J. C.; Magliozzo, R. S. Hydrogen peroxide-mediated isoniazid activation catalyzed by *Mycobacterium tuberculosis* catalase-peroxidase (KatG) and its S315T mutant. *Biochemistry* **2006**, *45*, 4131–4140.
- (29) Zhao, X.; Yu, S.; Magliozzo, R. S. Characterization of the binding of isoniazid and analogues to *Mycobacterium tuberculosis* catalase-peroxidase. *Biochemistry* **2007**, *46*, 3161–3170.
- (30) Metcalfe, C.; Macdonald, I. K.; Murphy, E. J.; Brown, K. A.; Raven, E. L.; Moody, P. C. The tuberculosis prodrug isoniazid bound to activating peroxidases. *J. Biol. Chem.* **2008**, *283*, 6193–6200.
- (31) Colin, J.; Wiseman, B.; Switala, J.; Loewen, P. C.; Ivancich, A. Distinct role of specific tryptophans in facilitating electron transfer or as [Fe (IV) = O Trp*] intermediates in the peroxidase reaction of *Burkholderia pseudomallei* catalase-peroxidase: A multifrequency EPR spectroscopy investigation. *J. Am. Chem. Soc.* **2009**, *131*, 8557–8563.
- (32) Zhao, X.; Hersleth, H.-P.; Zhu, J.; Andersson, K. K.; Magliozzo, R. S. Access channel residues Ser315 and Asp137 in *Mycobacterium tuberculosis* catalase-peroxidase (KatG) control peroxidatic activation of the pro-drug isoniazid. *Chem. Commun.* **2013**, *49*, 11650–11652.
- (33) Singh, R.; Wiseman, B.; Deemagarn, T.; Donald, L. J.; Duckworth, H. W.; Carpena, X.; Fita, I.; Loewen, P. C. Catalase-peroxidases (KatG) exhibit NADH oxidase activity. *J. Biol. Chem.* **2004**, *279*, 43098–43106.
- (34) Jakopitsch, C.; Auer, M.; Regelsberger, G.; Jantschko, W.; Furtmüller, P. G.; Rüker, F.; Obinger, C. Distal site aspartate is essential in the catalase activity of catalase-peroxidases. *Biochemistry* **2003**, *42*, 5292–5300.
- (35) Jakopitsch, C.; Droghetti, E.; Schmuckenschlager, F.; Furtmüller, P. G.; Smulevich, G.; Obinger, C. Role of the main access channel of catalase-peroxidase in catalysis. *J. Biol. Chem.* **2005**, *280*, 42411–42422.
- (36) Deemagarn, T.; Wiseman, B.; Carpena, X.; Ivancich, A.; Fita, I.; Loewen, P. C. Two alternative substrate paths for compound I formation and reduction in catalase-peroxidase KatG from *Burkholderia pseudomallei*. *Proteins: Struct., Funct., Genet.* **2007**, *66*, 219–228.
- (37) Machuqueiro, M.; Victor, B. L.; Switala, J.; Villanueva, J.; Rovira, C.; Fita, I.; Loewen, P. C. Catalase activity of catalase-peroxidases is modulated by changes in pK_a of the distal histidine. *Biochemistry* **2017**, *56*, 2271–2281.
- (38) Martins, F.; Santos, S.; Ventura, C.; Elvas-Leitão, R.; Santos, L.; Vitorino, S.; Reis, M.; Miranda, V.; Correia, H. F.; Aires-de-Sousa, J.; Kovalishyn, V.; Latino, D. A. R. S.; Ramos, J.; Viveiros, M. Design, synthesis and biological evaluation of novel isoniazid derivatives with potent antitubercular activity. *Eur. J. Med. Chem.* **2014**, *81*, 119–138.
- (39) Machado, D.; Perdigão, J.; Ramos, J.; Couto, I.; Portugal, I.; Ritter, C.; Boettger, E. C.; Viveiros, M. High-level resistance to isoniazid and ethionamide in multidrug-resistant *Mycobacterium tuberculosis* of the Lisboa family is associated with *inhA* double mutations. *J. Antimicrob. Chemother.* **2013**, *68*, 1728–1732.
- (40) Cambau, E.; Viveiros, M.; Machado, D.; Raskine, L.; Ritter, C.; Tortoli, E.; Matthys, V.; Hoffner, S.; Richter, E.; Perez Del Molino, M.; Cirillo, D. M.; van Soolingen, D.; Böttger, E. C. Revisiting susceptibility testing in MDR-TB by a standardized quantitative phenotypic assessment in a European multicentre study. *J. Antimicrob. Chemother.* **2015**, *70*, 686–696.
- (41) Machado, D.; Coelho, T. S.; Perdigão, J.; Pereira, C.; Couto, I.; Portugal, I.; Maschmann, R. D. A.; Ramos, D. F.; von Groll, A.; Rossetti, M. L.; Silva, P. A.; Viveiros, M. Interplay between Mutations and Efflux in Drug Resistant Clinical Isolates of *Mycobacterium tuberculosis*. *Front. Microbiol.* **2017**, *8*, 711.
- (42) Frisch, M. J.; et al. *Gaussian 09, Revision C.01*; Gaussian, Inc.: Wallingford, CT, 2009.
- (43) Zhao, Y.; Truhlar, D. G. *J. Chem. Theory Comput.* **2008**, *4*, 1849–1868.
- (44) Dunning, T. H., Jr Gaussian basis sets for use in correlated molecular calculations. I. The atoms boron through neon and hydrogen. *J. Chem. Phys.* **1989**, *90*, 1007–1023.
- (45) Kendall, R. A.; Dunning, T. H., Jr; Harrison, R. J. Electron affinities of the first-row atoms revisited. Systematic basis sets and wave functions. *J. Chem. Phys.* **1992**, *96*, 6796–6806.
- (46) Auclair, C.; Torres, M.; Hakim, J. Superoxide anion involvement in NBT reduction catalyzed by NADPH-cytochrome P-450 reductase: a pitfall. *FEBS Lett.* **1978**, *89*, 26–28.
- (47) Abraham, M. J.; Murtola, T.; Schulz, R.; Páll, S.; Smith, J. C.; Hess, B.; Lindahl, E. GROMACS: High performance molecular simulations through multi-level parallelism from laptops to supercomputers. *SoftwareX* **2015**, *1–2*, 19–25.
- (48) Scott, W. R. P.; Hünenberger, P. H.; Tironi, I. G.; Mark, A. E.; Billeter, S. R.; Fennel, J.; Torda, A. E.; Huber, T.; Krüger, P.; van Gunsteren, W. F. The GROMOS biomolecular simulation program package. *J. Phys. Chem. A* **1999**, *103*, 3596–3607.
- (49) van Gunsteren, W. F.; Daura, X.; Mark, A. E. *Encyclopedia of Computational Chemistry*; John Wiley & Sons, Ltd: 2002.
- (50) Schmid, N.; Eichenberger, A.; Choutko, A.; Riniker, S.; Winger, M.; Mark, A.; Van Gunsteren, W. Definition and testing of the GROMOS force-field versions 54A7 and 54B7. *Eur. Biophys. J.* **2011**, *40*, 843–856.
- (51) Hermans, J.; Berendsen, H. J. C.; van Gunsteren, W. F.; Postma, J. P. M. A Consistent Empirical Potential for Water-Protein Interactions. *Biopolymers* **1984**, *23*, 1513–1518.
- (52) Malde, A. K.; Zuo, L.; Breeze, M.; Stroet, M.; Poger, D.; Nair, P. C.; Oostenbrink, C.; Mark, A. E. An automated force field topology

builder (ATB) and repository: version 1.0. *J. Chem. Theory Comput.* **2011**, *7*, 4026–4037.

(53) Koziara, K. B.; Stroet, M.; Malde, A. K.; Mark, A. E. Testing and validation of the Automated Topology Builder (ATB) version 2.0: prediction of hydration free enthalpies. *J. Comput.-Aided Mol. Des.* **2014**, *28*, 221–233.

(54) Parrinello, M.; Rahman, A. Polymorphic transitions in single crystals: A new molecular dynamics method. *J. Appl. Phys.* **1981**, *52*, 7182–7190.

(55) Nosé, S.; Klein, M. Constant pressure molecular dynamics for molecular systems. *Mol. Phys.* **1983**, *50*, 1055–1076.

(56) Bussi, G.; Donadio, D.; Parrinello, M. Canonical sampling through velocity rescaling. *J. Chem. Phys.* **2007**, *126*, 014101.

(57) Hess, B. P-LINCS: A Parallel Linear Constraint Solver for Molecular Simulation. *J. Chem. Theory Comput.* **2008**, *4*, 116–122.

(58) Miyamoto, S.; Kollman, P. SETTLE: An analytical version of the SHAKE and RATTLE algorithm for rigid water models. *J. Comput. Chem.* **1992**, *13*, 952–962.

(59) Hub, J. S.; De Groot, B. L.; Van Der Spoel, D. *g_{wham}*: A Free Weighted Histogram Analysis Implementation Including Robust Error and Autocorrelation Estimates. *J. Chem. Theory Comput.* **2010**, *6*, 3713–3720.

(60) Diamond, J. M.; Katz, Y. Interpretation of nonelectrolyte partition coefficients between dimyristoyl lecithin and water. *J. Membr. Biol.* **1974**, *17*, 121–154.

(61) Marrink, S.-J.; Berendsen, H. J. Simulation of water transport through a lipid membrane. *J. Phys. Chem.* **1994**, *98*, 4155–4168.

(62) Hummer, G. Position-dependent diffusion coefficients and free energies from Bayesian analysis of equilibrium and replica molecular dynamics simulations. *New J. Phys.* **2005**, *7*, 34.

(63) Dickson, C. J.; Hornak, V.; Pearlstein, R. A.; Duca, J. S. Structure–Kinetic Relationships of Passive Membrane Permeation from Multiscale Modeling. *J. Am. Chem. Soc.* **2017**, *139*, 442–452.

(64) Wengenack, N. L.; Hoard, H. M.; Rusnak, F. Isoniazid Oxidation by Mycobacterium tuberculosis KatG: A Role for Superoxide Which Correlates with Isoniazid Susceptibility. *J. Am. Chem. Soc.* **1999**, *121*, 9748–9749.

(65) Ráfols, C.; Bosch, E.; Ruiz, R.; Box, K. J.; Reis, M.; Ventura, C.; Santos, S.; Araújo, M. E.; Martins, F. Acidity and hydrophobicity of several new potential antitubercular drugs: isoniazid and benzimidazole derivatives. *J. Chem. Eng. Data* **2012**, *57*, 330–338.